Vacuum electron acceleration and bunch compression by a flat-top laser beam

W. Wang
Applied Ion Beam Physics Laboratory, Key Laboratory of the Ministry of Education, Institute of Modern Physics, Fudan University, Shanghai, 200433, China and Shanghai Institute of Laser Plasma, Shanghai, 201800, China

P. X. Wang,[a] Y. K. Ho, and Q. Kong
Applied Ion Beam Physics Laboratory, Key Laboratory of the Ministry of Education, Institute of Modern Physics, Fudan University, Shanghai, 200433, China

Y. Gu and S. J. Wang
Shanghai Institute of Laser Plasma, Shanghai, 201800, China

(Received 17 June 2007; accepted 19 August 2007; published online 10 September 2007)

The field intensity distribution and phase velocity characteristics of a flat-top laser beam are analyzed and discussed. The dynamics of electron acceleration in this kind of beam are investigated using three-dimensional test particle simulations. Compared with the standard (i.e., TEM_{00} mode) Gaussian beam, a flat-top laser beam has a stronger longitudinal electric field and a larger diffraction angle. These characteristics make it easier for electrons to be trapped and accelerated by the beam. With a flat-top shape, the laser beam is also applicable to the acceleration of low energy electron and bunch compression. © *2007 American Institute of Physics.* [DOI: 10.1063/1.2780816]

I. INTRODUCTION

The development of new laser techniques[1] has stimulated research on the laser acceleration of particles.[2–9] In a previous work, we proposed the capture and acceleration scheme (CAS).[10] Those results were obtained using a TEM_{00} mode "standard Gaussian beam" (SGB). In this article, we report on a CAS using a flat-top laser beam, which is nearly uniform throughout a large central region of the focal plane. The beam intensity drops smoothly but quickly to zero outside this region, where a stronger longitudinal electric field, which is responsible for electron acceleration,[10] than that of SGB is expected. Note that this laser is not the same as the "focused flat-top beam" discussed in our prior work;[11] the latter is flat-top before being focused and exhibits side lobes in addition to the main spot. In this article, we analyze the electromagnetic field intensity distribution and phase velocity characteristics of an unaltered flat-top laser beam. Electron dynamics are investigated using three-dimensional (3D) test particle simulations.

To be effectively accelerated by a laser pulse, an electron should have quite high initial energy ($P_0 \sim 10$). Both experiments[12,13] and theory[14] indicate that low-energy electrons gain some energy from an intense laser pulse in vacuum. The net energy of the electrons cannot increase much, however, because the radial ponderomotive force quickly expels them from the beam. Recent research has constructed ponderomotive potential wells with π-shaped or even M-shaped radial profiles instead of the usual Gaussian profile, by making use of different order Hermite–Gaussian modes.[15,16] Electrons can be confined in the π-shaped potential well for a long time before leaving the laser beam. An intense combined laser pulse with a π-shaped potential well can drastically compress the electron bunch length.[16–18] However, it is almost impossible to obtain the high-order pure HG mode beam needed for constructing this π-shaped profile.[19]

Here we propose the flat-top laser beam as an alternative method of accelerating low-energy electrons. We use 3D test particle simulations to directly solve the relativistic Newton–Lorentz equation of motion, rather than working with the ponderomotive potential model.[16] Another goal of this article is to investigate the characteristics of low-energy electron acceleration and bunch compression pushed by a flat-top laser beam.

II. FLAT-TOP LASER BEAMS

One approach to describe beams with a flat-top profile is the flattened Gaussian beam (FGB) model introduced by Gori.[20] FGBs can be expressed as a superposition of N suitably weighted Laguerre–Gaussian (LG) beams. The FGB is therefore also a solution of the paraxial wave equation. The nonzero component of $\mathbf{A}$ ($A_x, A_y=0, A_z=0$) for a pulsed laser beam, polarized along the x direction and propagating in vacuum along the z axis, can be expressed within the paraxial wave approximation as

$$A_x = A_0 \frac{w_N(0)}{w_N} \exp\left(-\frac{r^2}{w_N^2}\right) \sum_{n=0}^{N} c_n^{(N)} L_n\left(\frac{2r^2}{w_N^2}\right) f(\eta) \cos[\varphi^{(p)} - 2n\varphi_N]. \quad (1)$$

The term $w_N(0)=w_0/\sqrt{N+1}$ represents the common LG

[a]Author to whom correspondence should be addressed; electronic mail: wpx@fudan.edu.cn

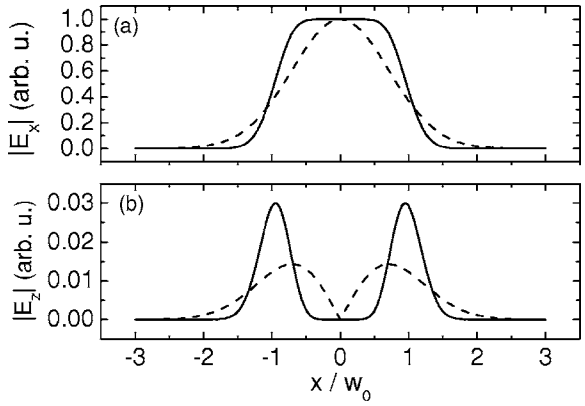

FIG. 1. Amplitude profiles of electric field components E_x (a) and E_z (b) in the waist planes of a SGB ($N=0$, dotted line) and FGB ($N=4$, solid line). Both laser beams are stationary, with beam waist $w_0=60$.

beam waist radius, so w_0 is the waist radius of the FGB. We also define the useful phase factor $\varphi^{(p)}=k\eta-\varphi_N-\varphi_0+kr^2/2R_N$. L_n is the nth Laguerre polynomial with amplitude $c_n^{(N)}=(-1)^n\sum_{m=n}^{N}\binom{m}{n}1/2^m$ where $\binom{m}{n}$ denotes the binomial coefficient. The propagation variables are $w_N=w_N(0)[1+(z/Z_R)^2]^{1/2}$, $R_N=z[1+(Z_R/z)^2]$, and $\varphi_N=\tan^{-1}(z/Z_R)$, where $Z_R=kw_N^2(0)/2$ is the Rayleigh length. The components of **E** and **B** can be derived by the relations $\mathbf{E}=-\partial\mathbf{A}/\partial t-\nabla\Phi$ and $\mathbf{B}=\nabla\times\mathbf{A}$ in the Lorentz gauge, as in our previous works.[11,21]

Amplitude profiles of the transverse and longitudinal electric field on the waist plane are shown in Fig. 1 for a SGB ($N=0$, dashed line) and a FGB ($N=4$, solid line). The laser beams are stationary and have a beam waist (kw_0) of 60 in both cases. The E_x profile is of course Gaussian for the $N=0$ (SGB) case, but the top of this curve flattens as N increases. The wings of the profile also become steeper. Note that the longitudinal electric field is approximately proportional to the partial derivative $\partial E_x/\partial x$ for a laser beam polarized along the x direction.[22] It is thus expected that a FGB will have a stronger longitudinal electric field near the beam edge.

Figure 2(b) shows the total intensity distribution of a FGB ($N=4$) in the x-z plane, with the "flat" region clearly visible in the center. The divergence profiles of the SGB ($N=0$, dashed line) and FGB ($N=4$, dash-dotted line) are also shown. Note that the FGB briefly widens as it propagates along the z axis, then narrows to a radius smaller than w_0 (the beam width at $z=0$) before diverging once more. At large distances, the FGB exhibits a larger diffraction angle than the SGB.

This unusual structure corresponds to the case of Fresnel diffraction by a circular aperture. The flatter the beam profile is in its waist plane (as N increases), the more evident this deformation becomes.[23] The diffraction angle of a FGB will be of concern to us, since it indicates the strength of the Fresnel diffraction effect. The diffraction generates regions of subluminous phase velocity in the beam. The scan lines of E_x intensity shown in Fig. 2(a) clearly show that the beam profile is either flat or slightly M shaped near the focus; this structure will help confine and accelerate the electrons.

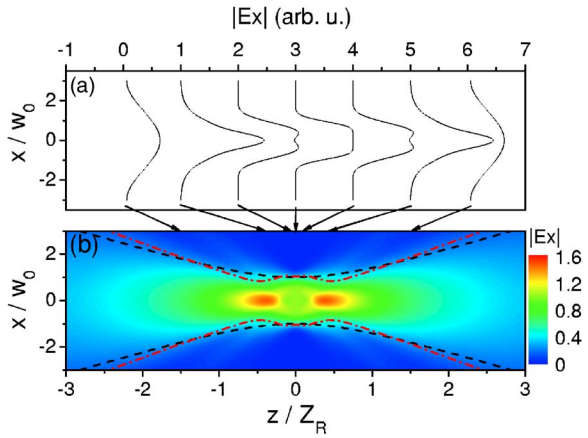

FIG. 2. (Color online) The distribution of beam intensity for a FGB ($N=4$). This laser beam has the same parameters as that shown in Fig. 1. (a) Cross-sectional intensity profiles at selected z. (b) The intensity distribution in the x-z plane. The dash-dotted and dashed lines show the FGB and SGB dispersion profiles, respectively.

The effective phase velocity $(V_\varphi)_l$ of the wave along a particle trajectory can be calculated using the relation $\partial\varphi/\partial t+(V_\varphi)_l(\nabla\varphi)_l=0$ The phase of the wave is given by φ, and $(\nabla\varphi)_l$ is the component of the phase gradient along the particle trajectory.[10] The minimum phase velocity, which is normally called the phase velocity of the wave, can be expressed as $V_p=-(\partial\varphi/\partial t)/|\nabla\varphi|$. Figure 3 shows distributions of the minimum phase velocity (in units of c) near the beam waist for the SGB (a) and FGB (b). The dash-dotted lines in Fig. 3(b) indicate the divergence profile of the FGB beam. Two regions with a subluminous phase velocity are evident near the focus of the FGB distribution, which is quite unlike the SGB distribution. This complex structure is entirely due to the diffraction effect. In the $N=0$ (SGB) case, the subluminous region lies beyond the beam width $w(z)$. In the $N=4$ (FGB) case, the subluminous region is broken up but for the most part occupies a similar domain. Given the strong longitudinal electric field of the FGB, however, it is reasonable to expect that the CAS remains valid despite these differences.

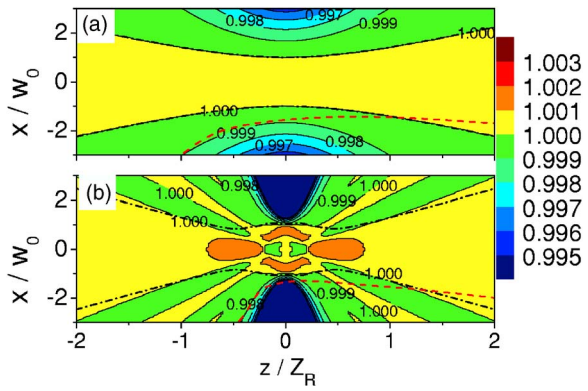

FIG. 3. (Color online) The minimum phase velocity V_p (in units of c) of (a) a SGB ($N=0$) and (b) a FGB ($N=4$). The parameters of both beams are as in Fig. 1. Dash-dotted lines show the beam divergence profiles. The dashed lines trace a typical electron trajectory in the capture and acceleration scheme.

III. ELECTRON DYNAMICS IN A FGB

The dynamics of electrons in a FGB ($N=4$) propagating in vacuum are investigated using 3D test particle simulations. We numerically solve the relativistic Newton–Lorentz equation[10] $d\mathbf{P}/dt=-e(\mathbf{E}+\mathbf{v}\times\mathbf{B})$, where $\mathbf{v}$ is the electron velocity, $\mathbf{P}=\gamma\mathbf{v}$ is the electron momentum in units of $m_e c$, and γ is the Lorentz factor. The simulations are performed at laser intensity $a_0=30$, where $a_0\equiv eE_0/m_e\omega c$ is a dimensionless parameter. E_0 denotes the electric field amplitude at the focus and ω is the laser's angular frequency. Throughout this article, time and length are expressed in units of $1/\omega$ and $1/k$. The beam width at the focus is $w_0=60$ and the laser pulse duration is $\tau=500$. The electrons are given an initial momentum $P_0=6$ directed toward the origin with incident crossing angle $\theta=\tan^{-1}0.22$. (Electrons with initial conditions in the approximate ranges $P_0=5-10$, $\tan\theta=0.15-0.3$, and $1.25<P_0\tan\theta<1.7$ can be captured and accelerated effectively.)

Varying the laser's initial phase from 0 to 2π, we find that a large fraction of incident electrons are accelerated effectively just as in the SGB ($N=0$) case.[10] When an electron is captured, the effective phase velocity of the electromagnetic wave can approach c along the dynamic trajectory of the captured particle. It can even approach the speed of the particle itself.[10] A captured electron can thus be kept in the acceleration phase of the wave for long time and gain considerable energy from the laser field. Note that in a CAS the longitudinal electric field is responsible for the energy gain. Electrons in a FGB experience a high longitudinal force at the edges of the flat region, and gain more energy than they would in a SGB. The results of these simulations indicate that the CAS holds in a FGB.

The optimal incident angle of an electron in the FGB case is also significantly larger than in the SGB case. This result is also useful, since incoming electrons need not meet the lens and CAS experiments will be easier to carry out.

IV. ELECTRON BUNCH COMPRESSION IN A FGB

When a laser beam with a radial Gaussian profile pushes low-energy electrons, off-axis electrons experience a strong radial ponderomotive force and are quickly expelled from the beam. This prevents them from gaining much energy. Using a FGB may overcome this problem, because there is almost no radial ponderomotive force in the uniform central region. In this section we investigate the characteristics of low-energy electron acceleration and violent bunch compression in our 3D test particle simulations. The geometry of electron acceleration is the same as that given in Ref. 16.

Figure 4 shows the final Lorentz factor γ_f and scattering angle of initially on-axis ($x_0=y_0=0$) electrons accelerated by a FGB with $N=8$ This simulation's laser parameters are as follows: laser intensity $a_0=10$, beam width $kw_0=100$, and pulse duration $\omega\tau=500$. The initial momentum of the electrons is $P_x=P_y=0$, $P_z=0.05$. Without the influence of the laser field, an electron with $\Delta t=0$ is expected to arrive at the origin ($x=y=z=0$) at the same time ($t=0$) as the laser beam. If $|\Delta t|$ is large enough, the electron experiences a negligible laser field and travels straight ahead. For lower values of $|\Delta t|$, electrons are quickly expelled from the beam with a large scattering angle and cannot gain much energy. For very small values of $|\Delta t|$, electrons remain in the beam and are effectively accelerated.

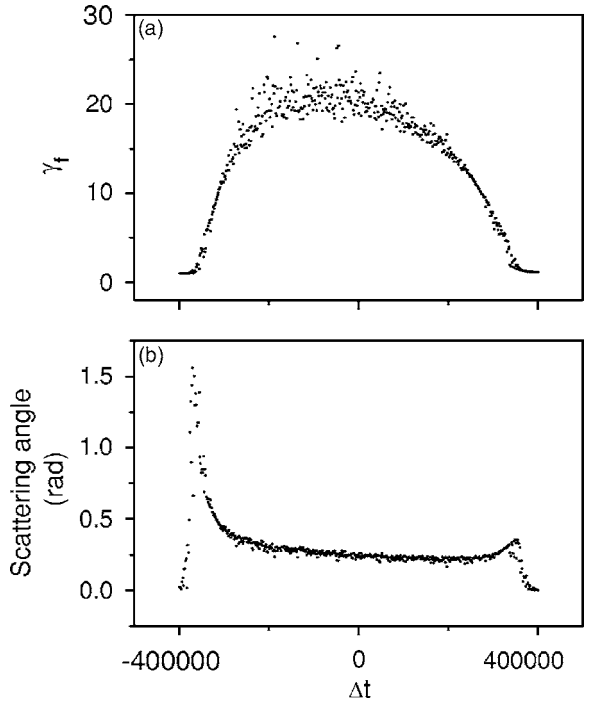

FIG. 4. The final energy (a) and scattering angle (b) of initially on-axis ($x_0=y_0=0$) electrons accelerated by a flat-top laser beam with $N=8$, laser intensity $a_0=10$, beam width $kw_0=100$, and pulse duration $\omega\tau=500$. The initial momentum is $P_x=P_y=0$, $P_z=0.05$ for all electrons. Without the influence of the laser field, an electron with $\Delta t=0$ will reach the origin ($x=y=z=0$) at the same time ($t=0$) as the laser beam.

Figure 5 demonstrates the longitudinal compression of initially on-axis ($x_0=y_0=0$) electrons in a FGB with $N=8$. The parameters of this simulation are the same as in Fig. 4.

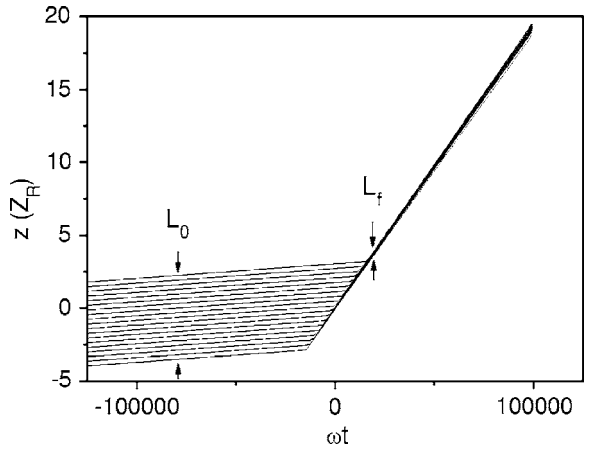

FIG. 5. The longitudinal compression of initially on-axis ($x_0=y_0=0$) electrons by a flat-top laser beam with $N=8$, laser intensity $a_0=10$, beam width $kw_0=100$, and pulse duration $\omega\tau=500$. The initial momentum is $P_x=P_y=0$, $P_z=0.05$ for all electrons. L_0 and L_f are the initial and final electron bunch length, respectively.

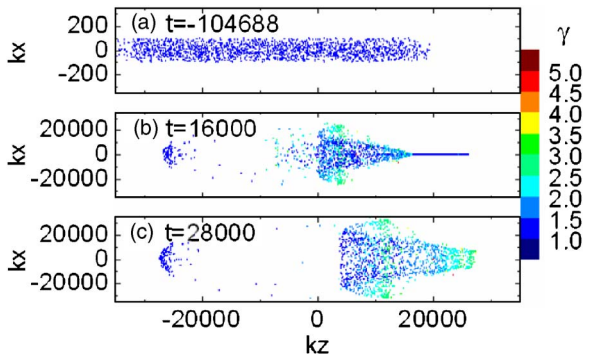

FIG. 6. (Color online) Snapshots of a uniformly distributed, cylindrical electron bunch accelerated and compressed by a flat-top laser beam. The bunch is visualized at $t=-104\,688$ (a), 16 000 (b), and 28 000 (c). The beam parameters are $N=8$, laser intensity $a_0=10$, beam width $kw_0=100$, and pulse duration $\omega\tau=500$. The initial momentum is $P_x=P_y=0$ and $P_z=0.05$ for all electrons. The color scale shows the electron energy.

L_0 and L_f are the initial and final bunch length, respectively. L_0 is the maximum length attained by the electron bunch before compression and increases with kw_0 Theoretically, the compression ratio of electrons accelerated from v_0 to v can be expressed as $L_0/L_f=(c-v_0)/(c-v)$. If v is close to c and $v_0 \ll c$, the compression ratio will obviously be quite high. In the case of Fig. 5, it is 200. In contrast, the typical compression ratio of a magnetic bunch compressor is only 4–5.[24,25]

Finally, a cylinder-shaped electron bunch is simulated to highlight the compression properties of the beam for off-axis electrons. Three snapshots taken at different times are shown in Fig. 6, where the color scale indicates electron energy. The initial momentums are all $P_x=P_y=0$ and $P_z=0.05$, and the electrons are uniformly distributed in a cylinder of radius w_0. The cylinder is coaxial with the laser beam. The simulation parameters are $N=8$ (FGB), laser intensity $a_0=10$, beam width $kw_0=100$, and pulse duration $\omega\tau=500$. If we consider only the forward region with high final energy, the electron bunch has been longitudinally compressed by a factor of ~ 10. This is much lower than the on-axis case.

V. DISCUSSION

We have analyzed the field structure and electron acceleration scheme of an intense laser beam with a flattened Gaussian profile (FGB). The longitudinal electric field of a FGB is stronger than that of a standard Gaussian beam, and its diffraction angle is larger. The first characteristic means that an FGB can accelerate electrons to higher energy, and the second allows electrons to be injected with larger crossing angles. The FGB is quite practical for low-energy electron acceleration and bunch compression. Simulations show that an electron bunch with uniform distribution can be accelerated to relativistic speeds. An extremely high longitudinal compression factor is also evident in the results. Although the final energy of the electrons is not as high as that produced by other schemes, this method has some advantages and may find a useful application in fast ignition fusion.

ACKNOWLEDGMENTS

This work is supported partly by National Natural Science Foundation of China under contract Nos. 10475018 and 10335030 and the National High-Tech ICF Committee of China.

[1] M. Aoyama, K. Yamakawa, Y. Akahane, J. Ma, N. Inoue, H. Ueda, and H. Kiriyama, Opt. Lett. **28**, 1594 (2003); S.-W. Bahk, P. Rousseau, T. A. Planchon, V. Chvykov, G. Kalintchenko, A. Maksimchuk, G. A. Mourou, and V. Yanovsky, *ibid.* **29**, 2837 (2004); S.-W. Bahk, P. Rousseau, T. A. Planchon, V. Chvykov, G. Kalintchenko, A. Maksimchuk, G. A. Mourou, and V. Yanovsky, Appl. Phys. B: Lasers Opt. **80**, 823 (2005).
[2] T. Tajima and G. Mourou, Phys. Rev. ST Accel. Beams **5**, 031301 (2002).
[3] S. P. D. Mangles, C. D. Murphy, Z. Najmudin, A. G. R. Thomas, J. L. Collier, A. E. Dangor, E. J. Divall, P. S. Foster, J. G. Gallacher, C. J. Hooker, D. A. Jaroszynski, A. J. Langley, W. B. Mori, P. A. Norreys, F. S. Tsung, R. Viskup, B. R. Walton, and K. Krushelnick, Nature (London) **431**, 535 (2004); C. G. R. Geddes, Cs. Toth, J. van Tilborg, E. Esarey, C. B. Schroeder, D. Bruhwiler, C. Nieter, J. Cary, and W. P. Leemans, *ibid.* **431**, 538 (2004); J. Faure, Y. Glinec, A. Pukhov, S. Kiselev, S. Gordienko, E. Lefebvre, J.-P. Rousseau, F. Burgy, and V. Malka, *ibid.* **431**, 541 (2004).
[4] Y. I. Salamin and C. H. Keitel, Phys. Rev. Lett. **88**, 095005 (2002); Y. I. Salamin and C. H. Keitel, Appl. Phys. Lett. **77**, 1082 (2000); Y. I. Salamin, Phys. Lett. A **335**, 289 (2005).
[5] T. Ohkubo, A. Maekawa, R. Tsujii, T. Hosokai, K. Kinoshita, K. Kobayashi, M. Uesaka, A. Zhidkov, K. Nemoto, Y. Kondo, and Y. Shibata, Phys. Rev. ST Accel. Beams **10**, 031301 (2007).
[6] T. Plettner, P. P. Lu, and R. L. Byer, Phys. Rev. ST Accel. Beams **9**, 111301 (2006); T. Plettner, R. L. Byer, E. Colby, B. Cowan, C. M. S. Sears, J. E. Spencer, and R. H. Siemann, *ibid.* **8**, 121301 (2005).
[7] V. Malka, A. Lifschitz, J. Faure, and Y. Glinec, Phys. Rev. ST Accel. Beams **9**, 091301 (2006).
[8] W. Yu, V. Bychenkov, Y. Sentoku, M. Y. Yu, Z. M. Sheng, and K. Mima, Phys. Rev. Lett. **85**, 570 (2000).
[9] B. M. Hegelich, B. J. Albright, J. Cobble, K. Flippo, S. Letzring, M. Paffett, H. Ruhl, J. Schreiber, R. K. Schulze, and J. C. Fernandez, Nature (London) **439**, 441 (2006); H. Schwoerer, S. Pfotenhauer, O. Jackel, K.-U. Amthor, B. Liesfeld, W. Ziegler, R. Sauerbrey, K. W. D. Ledingham, and T. Esirkepov, *ibid.* **439**, 445 (2006); T. Toncian, M. Borghesi, J. Fuchs, E. d'Humières, P. Antici, P. Audebert, E. Brambrink, C. A. Cecchetti, A. Pipahl, L. Romagnani, and O. Willi, Science **312**, 410 (2006).
[10] P. X. Wang, Y. K. Ho, X. Q. Yuan, Q. Kong, N. Cao, A. M. Sessler, E. Esarey, and Y. Nishida, Appl. Phys. Lett. **78**, 2253 (2001).
[11] W. Wang, P. X. Wang, Y. K. Ho, Q. Kong, Z. Chen, Y. Gu, and S. J. Wang, Europhys. Lett. **73**, 211 (2006); Appl. Phys. B: Lasers Opt. **88**, 273 (2007).
[12] G. Malka, E. Lefebvre, and J. L. Miquel, Phys. Rev. Lett. **78**, 3314 (1997); **80**, 1352 (1998).
[13] C. I. Moore, J. P. Knauer, and D. D. Meyerhofer, Phys. Rev. Lett. **74**, 2439 (1995); P. H. Bucksbaum, M. Bashkansky, and T. J. McIlrath, *ibid.* **58**, 349 (1987); P. Monot, T. Auguste, L. A. Lompre', G. Mainfrary, and C. Manus, *ibid.* **70**, 1232 (1993); Y. I. Salamin and C. H. Keitel, Appl. Phys. Lett. **77**, 1082 (2000).
[14] E. S. Sarachik and G. T. Schappert, Phys. Rev. D **1**, 2738 (1970); P. K. Kaw and R. M. Kulsrud, Phys. Fluids **16**, 321 (1973); W. Scheild and H. Hora, Laser Part. Beams **7**, 315 (1989).
[15] G. V. Stupakov and M. S. Zolotorev, Phys. Rev. Lett. **86**, 5274 (2001).
[16] P. X. Wang, Ch. X. Tang, and Sh. J. Huang, Appl. Phys. Lett. **82**, 2752 (2003); Sh. J. Huang, Ch. X. Tang, and P. X. Wang, J. Appl. Phys. **95**, 2163 (2004).
[17] Q. Kong, S. Miyazaki, S. Kawata, K. Miyauchi, K. Nakajima, S. Masuda, N. Miyanaga, and Y. K. Ho, Phys. Plasmas **10**, 4605 (2003); Q. Kong, S. Miyazaki, S. Kawata, K. Miyauchi, K. Sakai, Y. K. Ho, K. Nakajima, N. Miyanaga, J. Limpouch, and A. A. Andreev, Phys. Rev. E **69**, 056502 (2004).
[18] S. Kawata, Q. Kong, S. Miyazaki, K. Miyauchi, R. Sonobe, K. Sakai, K. Nakajima, S. Masuda, Y. K. Ho, N. Miyanaga, J. Limpouch, and A. A. Andreev, Laser Part. Beams **23**, 61 (2005); S. Miyazaki, S. Kawata, Q. Kong, K. Miyauchi, K. Sakai, S. Hasumi, R. Sonobe, and T. Kikuchi, J. Phys. D **38**, 1665 (2005).

[19] A. E. Siegman, *Lasers* (University Science Books, Mill Valley, CA, 1986), p. 648.
[20] F. Gori, Opt. Commun. **107**, 335 (1994).
[21] P. X. Wang and J. X. Wang, Appl. Phys. Lett. **81**, 4473 (2002).
[22] M. Lax, W. H. Louisell, and W. B. McKnight, Phys. Rev. A **11**, 1365 (1975); L. W. Davis, *ibid.* **19**, 1177 (1979).
[23] V. Bagini, R. Borghi, F. Gori, A. M. Pacileo, M. Santarsiero, D. Ambrosini, and G. Schirripa, J. Opt. Soc. Am. A **13**, 1385 (1996).
[24] M. Geitz, A. Kabel, G. Schmidt, and H. Weise, Proceedings of the 1999 Particle Accelerator Conference, New York, 1999, p. 2507.
[25] A. Loulergue and A. Mosnier, Proceedings of EPAC, Vienna, Austria, 2000, p. 752.